Article

Bull. Volcanol. Soc. Japan
Vol. 58 (2013) No. 1, pp. 251−267

Shallow Resistivity Structure of Sakurajima Volcano Revealed by Audio-frequency Magnetotellurics

Wataru KANDA[1], Tomoya YAMAZAKI[2], Yasuo OGAWA[1], Takeshi HASHIMOTO[3], Shin'ya SAKANAKA[4], Koki AIZAWA[5,10], Shinichi TAKAKURA[6], Takao KOYAMA[5], Kenta YAMADA[4], Tsukasa KOBAYASHI[7] and Shogo KOMORI[8,9]

(Received October 5, 2011; Accepted April 27, 2012)

An audio-frequency magnetotelluric (AMT) survey was conducted at the foot of Sakurajima volcano in November 2007. This survey was carried out within the framework of the 7th National Project for Prediction of Volcano Eruptions. The main objective was to clarify the shallow layers of Sakurajima volcano for better understanding of the volcanic activity. We measured electromagnetic fields at frequencies from 1 to 10400 Hz at 27 locations along only three lines set on the northern, western, and southeastern flanks of the volcano. The three profiles enclosed the summit area where access is prohibited because of frequent explosive vulcanian eruptions. The data quality was generally considered to be good at frequencies higher than 2 Hz. Two-dimensional and three-dimensional (3-D) modeling approaches were applied to the data.

As a result of 3-D modeling, we obtained the following features in the resistivity model. The surface layer showed a high resistivity from several hundreds to thousands of ohm-meters and corresponded to the lava. This surface layer covered a highly conductive layer with a resistivity of less than tens of ohm-meters, interpreted as containing seawater or groundwater. However, the basement structure was not clearly detected, except for in an area of northern Sakurajima. The first lava layer was distributed thickly in northern and western parts of Sakurajima, and the boundary between the first and second layers was typically located at around sea level.

The conductive second layer was found at deeper levels beneath areas such as the Haruta-yama lava dome and the Nabe-yama pumice cone. This depression of the low resistivity layer is probably caused by the fracture zone associated with previous eruptions, which is formed above the conductive layer. In the proximity of Hikino-hira lava dome and the Taisho crater, the second conductive layer was found at a depth shallower than sea level, suggesting that a hydrothermal system has developed underneath this area. In contrast, elevation of the second layer was not seen on the side of Taisho crater located nearest to the edge of Nabe-yama, implying that a heat source is not present beneath the eastern foot of Sakurajima.

Key words: Sakurajima volcano, electrical resistivity structure, hydrothermal system, flank eruption, prediction of volcanic eruptions

[1] Kusatsu-Shirane Volcano Observatory, Volcanic Fluid Research Center, Tokyo Institute of Technology, 641−36 Kusatsu, Agatsuma, Gunma 377−1711, Japan.
[2] Disaster Prevention Research Institute, Kyoto University, Gokasho, Uji, Kyoto 611−0011, Japan.
[3] Faculty of Science, Hokkaido University, N10W8, Kita-ku, Sapporo 060−0810, Japan.
[4] Graduate School of Engineering and Resource Science, Akita University, 1−1 Tegata gakuen-machi, Akita 010−8502, Japan.
[5] Earthquake Research Institute, the University of Tokyo, 1−1−1, Yayoi, Bunkyo-ku, Tokyo 113−0032, Japan.
[6] National Institute of Advanced Industrial Science and Technology (AIST), Tsukuba West, 16−1 Onogawa, Tsukuba, Ibaraki 305−8569, Japan.
[7] Maizuru Marine Observatory, Japan Meteorological Agency, 901 Shimofukui, Maizuru, Kyoto 624−0946, Japan.
[8] Aso Volcanological Laboratory, Graduate School of Science, Kyoto University, Minami-Aso, Kumamoto 869−1404, Japan.
[9] Now: Institute of Earth Sciences, Academia Sinica, 128 Academia Road, Section 2, Nankang, Taipei 115, Taiwan.
[10] Now: Institute of Seismology and Volcanology, Faculty of Sciences, Kyushu University, 2−5643−29 Shin'yama, Shimabara, Nagasaki 855−0843, Japan.

Corresponding author: Wataru Kanda
e-mail: kanda@ksvo.titech.ac.jp

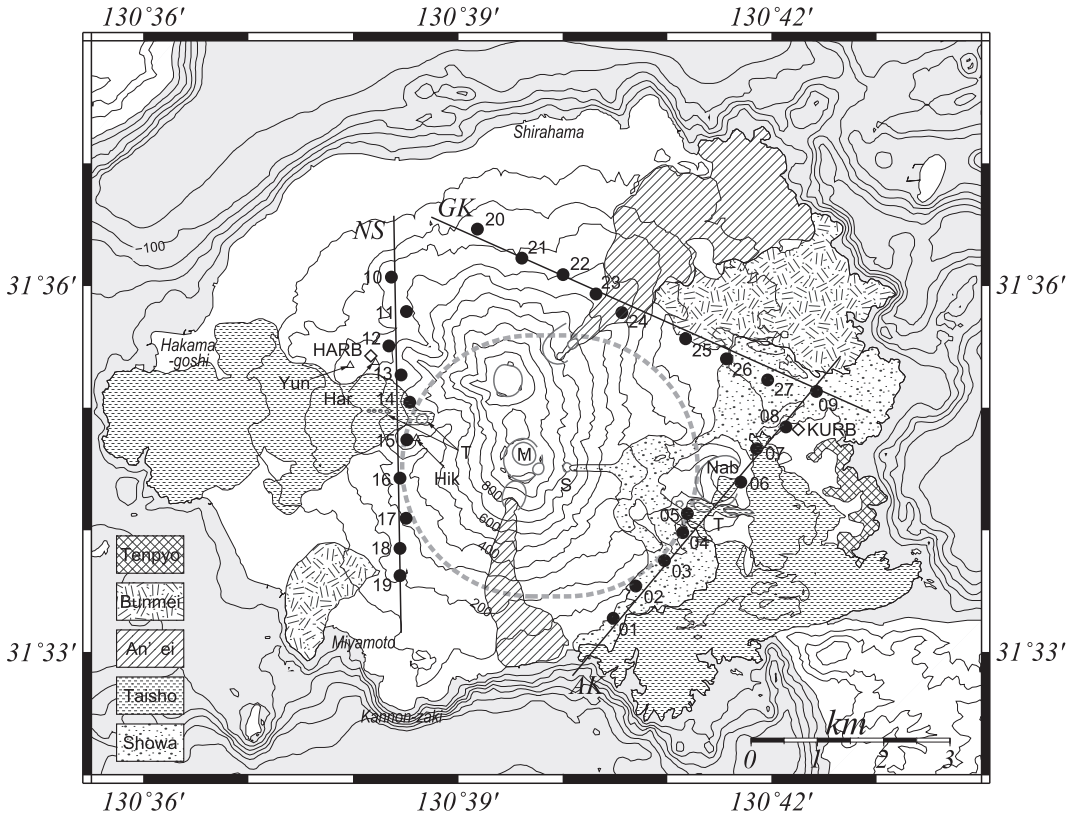

Fig. 1. Map of AMT site. Three solid lines indicate measurement lines (AK, NS, and GK) used in the analysis. Note that both AK and GK lines include site 09. Open diamonds denote the position of boreholes (HARB and KURB) referred to in the interpretation. The main craters and lava distributions from different historic ages (Fukuyama and Ono, 1981) are represented by gray outlines and hachure patterns, respectively. A dashed line indicates the 2 km off-limits boundary from Minami-dake (M) and the Showa (S) craters. Lava domes are indicated by open triangles (Hik: Hikino-hira; Har: Haruta-yama; Yun: Yuno-hira). Other geographical features (Nab: Nabe-yama pumice cone; T: Taisho crater) and the local name of places (Shirahama, Hakamagoshi, Miyamoto, and Kannon-zaki) are also labeled.

1. Introduction

This paper describes an outline and various results from audio-frequency magnetotelluric (AMT) surveys conducted as a part of the 10th Joint Observation of Sakurajima Volcano in 2007. At Sakurajima, continuous volcanic activity at the summit of Minami-dake has occurred since 1955 (Japan Meteorological Agency, 2005, p. 546). Repeated leveling surveys around Sakurajima have revealed an inflating tendency for the ground deformation since the Taisho eruption in 1914 (Eto, 1967; Kamo and Ishihara, 1980); however, in the late 1980's this tendency swapped to a deflating one, because eruption activities were accompanied by a large amount of ash ejection at the summit. In the early 1990's the eruption activity declined, and the ground resumed a process of upheaval (Eto *et al.*, 1997) that continues to the present. This upheaval implies that magma has accumulated in the reservoir that is thought to exist beneath the Aira caldera (Iguchi, 2006). From around 2001, volcanic activity in the region has been at a low level. Subsequently, after 58 years of dormancy, an eruption occurred at the Showa crater (S in Fig. 1) that is located a few hundred meters east of the Minami-dake crater (M in Fig. 1) in June 2006, and explosive eruption activities in the Showa crater have been continued since (Iguchi *et al.*, 2010).

Although the primary volcanic activity for the past 50 years has been explosive eruptions from the summit crater of Minami-dake, in historic ages (Tenpyo-Hoji, in 764; Bunmei, in 1471–1476; An'ei, in 1779; and Taisho, in 1914–1915) large amounts of lava were effused several times at the flanks of the volcano (Fukuyama and Ono, 1981). Each of these flank eruptions produced clusters of craterlets that are distributed mostly along a line passing through the Minami-dake summit; however the direction

of each line is different. This difference suggests that local stress fields at shallow depths act in a different manner from the regional stress field around Sakurajima. From the vertical discontinuities in the occurrence frequency of A-type earthquakes and in the source mechanism of those earthquakes, Ishihara (1988) proposed that a structural boundary is present at a depth of about 2 km beneath Minami-dake. He considered that the magma is temporarily stored around the structural boundary and that the pressure changes at this position control the local stress field at depths shallower than 2 km. To investigate this hypothesis further, information on the shallow structure is essential.

Furthermore, the shallow layer of a volcano can induce a diversity of volcanic activity (*e.g.*, Kagiyama, 2008). In particular, the existence of groundwater is related directly to the occurrence of dangerous phreatomagmatic explosions (*e.g.*, Kagiyama *et al.*, 1999), and this can cause increasing flank instability through hydrothermal activity (*e.g.*, Reid, 2004). Surveying the distribution of the groundwater layer around the crater of a flank eruption that has effused large amounts of lavas and pumices can contribute to the evaluation of such volcanic hazards. Measurement of underground resistivity is a promising method of investigating the groundwater layer or the hydrothermally altered layer resulting from circulation of volcanic fluids (*e.g.*, Kagiyama *et al.*, 1999; Finizola *et al.*, 2006; Aizawa *et al.*, 2009).

However, sufficient information has not been acquired in previous works. The electrical resistivity distribution at Sakurajima has been investigated from the 3rd Joint Observation Campaign to the 9th Campaign (Yukutake *et al*., 1980; Tanaka *et al*., 1982; 1986; Nishimura *et al*., 1988; 1989; Karohji *et al*., 1989; Kubota *et al*., 1995; Yamazaki *et al*., 1998). In addition, Kakioka Magnetic Observatory belonging to the Japan Meteorological Agency carried out resistivity surveys as part of routine monitoring of the volcanic activity (Tokumoto *et al*., 1988; Fukushima *et al*., 1988; 1989). The main objective of these observations was to detect resistivity changes associated with volcanic activity. Therefore, electrical methods were predominantly used in these studies such as dipole−dipole methods or magnetotelluric (MT) methods in which the measuring frequency was limited to 8−30 Hz. Recently, Aizawa *et al*. (2011) investigated a temporal change in the resistivity structure of Sakurajima, found from the continuous MT observation using a broadband frequency for a period of one year, and discussed the relation between this change and corresponding volcanic activity. However, since they used only two sites, sufficient information on the structure of Sakurajima has yet to be acquired.

In this study, we set three measurement lines on the flanks of the volcano and carried out AMT measurements (Fig. 1). Since the frequency range used in the present study was from 1 to 10400 Hz, the resistivity structure from the surface up to depths of 1−2 km, which have not been clarified in previous studies, can be estimated. The principal objective of the present study was to elucidate the shallow layers of Sakurajima's electrical resistivity structure, and to obtain structural information about the conditions under which flank eruptions took place.

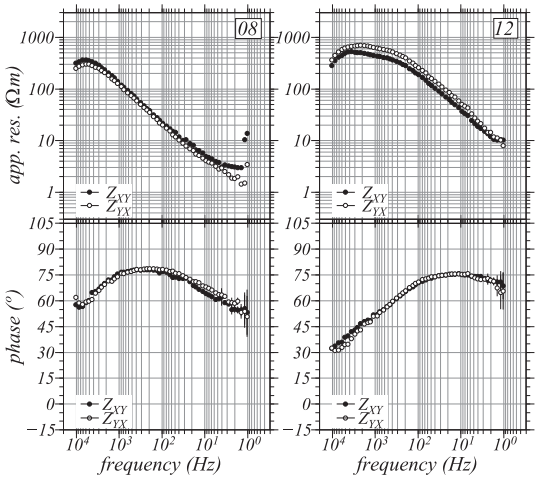

Fig. 2. Typical sounding curves of measured AMT data obtained at sites 08 and 12. The apparent resistivity (app. res.; upper plots) and the phase (lower plots) computed from the Z_{XY}-component (black dots) and from the Z_{YX}-component (white dots) are shown. Note that the Z_{YX}-component of phase is expressed through a rotation of 180°.

2. AMT observation and data

2−1 Outline of the observation

We carried out an AMT survey from 30 October through to 4 November 2007. The off-limits area at Sakurajima volcano is defined as being less than 2 km from the Minami-dake summit crater or from the Showa crater, both of which repeatedly have explosive eruptions. As a result of this restriction, designing a measurement line across the summit area is difficult, because there is no route that passes through the central part of the volcano. As a result, we conducted electromagnetic field measurements at 27 locations on the flanks of the volcano along three lines (AK, GK, and NS in Fig. 1) enclosing the volcanic edifice.

To take the measurements, a total of seven MTU-5A systems (Phoenix Geophysics Ltd., Canada) were used and data were recorded during the nighttime (20: 00 to 06: 00 local time). Since data synchronized by a GPS clock were obtained at five or six sites in a night, mutual local reference processing was performed.

2−2 Data

In Fig. 2, examples of typical sounding curves for the apparent resistivity and phase are shown for two sites. The

data quality was considered to be good in the frequency range from 2 Hz to values in the thousands of hertz, except for at a small number of sites. At almost all sites, we see a tendency for the apparent resistivities to decrease monotonically from hundreds of ohm-meters to less than tens of ohm-meters as the frequency decreases. In phase curves, an increasing trend from phases of 30°−50° to phases exceeding 70° is commonly seen as the frequency reduces. However, differences are found in the low frequencies of the phase curves site-by-site. For example, although the phase decreases at low frequencies for sites along the AK line on the southeastern flank of the volcano, this tendency is not as marked along the NS line on the western flank and high phases are maintained (Fig. 2).

At certain sites, we see that the phase rapidly increases at the highest frequencies (7000−10400 Hz) and that, conversely, the apparent resistivity decreases. This inverse relation is caused not by a conductor of the uppermost layer but by a low-pass filter built into the MTU-5A system. When the ground resistance reaches levels of tens of thousands of ohms, such data are often obtained. Since fitting a resistivity model to these areas is unfeasible, the associated data were removed in the modeling process described later.

2−3 Distribution of apparent resistivity and induction arrows

To obtain a rough understanding of the entire dataset, we calculated the apparent resistivity based on a rotational invariant of the impedance tensor. Fig. 3 shows the spatial distribution of the apparent resistivity for six characteristic frequencies calculated from the rotational invariant det(Re(**Z**)), which is thought to be a quantity that reflects the three-dimensional (3-D) distribution of the conductors appropriately (Szarka and Menvielle, 1997).

The trend in Fig. 3 matches that already shown in the sounding curves (Fig. 2); namely, the apparent resistivity decreases as the frequency becomes low. At these lower frequencies (＜100 Hz), areas of comparatively high resistivity are found along each survey line; an area over which An'ei lava is distributed on the GK line (sites 22, 23, and 24), a surrounding area of Nabe-yama on the AK line (sites 05, 06, and 07), and an area north of the Taisho crater (T in Fig. 1) on the NS line (sites 12 and 13). In contrast, an area from the Taisho crater to Hikino-hira, a lava dome on the western flank, is relatively conductive (sites 14 and 15).

In Fig. 3, the distribution of the real induction arrows (Parkinson, 1962) is additionally shown. The induction vector has properties that indicate contrasts in lateral resistivity and the vector will point in the direction of a conductive region. However, vectors tend to point toward a topographically high region at frequencies above about 100 Hz, even if there is no good conductor in the area (Müller and Haak, 2004). At 1100 and 530 Hz, the induction vectors along the AK and GK lines primarily point toward the central part of the volcano (Fig. 3), and we assume this to be as a consequence of this topographic effect. This tendency becomes weaker at a frequency of about 100 Hz, and the arrows instead reflect the resistivity contrast of the underground structure. At 49 Hz, the vectors at a number of sites point toward the sea, which is a good conductor, and this trait is even more pronounced at lower frequencies. However, at frequencies of less than 10 Hz, the induction vectors at some sites along the NS line (sites 11, 13, 15, 16, and 17) point in the direction of Minami-dake, suggesting the existence of another good conductor beneath Minami-dake.

3. Dimensionality and strike

Calculating the phase-sensitive skew (a measure of dimensionality), we found that this was less than 0.3 for almost all usable data at all sites. Thus, we can presume that the subsurface structure in this region is one-dimensional (1-D) or two-dimensional (2-D) and can, accordingly perform a 2-D analysis (Bahr, 1988). To this end, first, the strike directions for this 2-D analysis were estimated from individual impedance data by using a tensor decomposition technique (hereinafter referred to as GBD; Groom and Bailey, 1989). Polar histograms of strike estimates for frequency-dependent and site-dependent decompositions are shown in Fig. 4 for each line.

Strike estimates from data along the AK line (Fig. 4(a)) are principally in the N0° W−N10° W direction (or N80° E−N90° E direction). The histograms of strikes estimated for data along the NS and GK lines (Figs. 4(b) and (c)) also show a dominant direction of nearly N−S (or E−W). Since Sakurajima volcano has grown in a regional stress field with an approximately E−W extension (Hayasaka, 1987), the underground structure of Sakurajima is considered to have a directional property with an approximately N−S strike.

We recognize that the second dominant direction is around N30° E (or N60° W) in the NS and GK lines. In Figs. 4(d)−(f), histograms of strike estimates obtained from data at frequencies lower than 10 Hz are shown for each line. In the GK line (Fig. 4(f)), the estimated strikes are concentrated between N15° E and N30° E (or between N60° W and N75° W). This feature is also seen in the AK and NS lines (Figs. 4(d) and (e)), although the concentration is not remarkable. The induction arrows at frequencies lower than 10 Hz at many of sites located in the eastern region of Sakurajima tend to point in a southeast direction (Fig. 3). The presence of a resistivity contrast is suggested by the direction of the arrows, and hence, the strike direction is roughly presumed to be northeast. These results indicate the possibility that the direction of the 2-D strike or the dimensionality of the structure differs with depth, and suggest that a simple 2-D analysis is difficult to perform.

As a preliminary analysis we applied a 2-D inversion

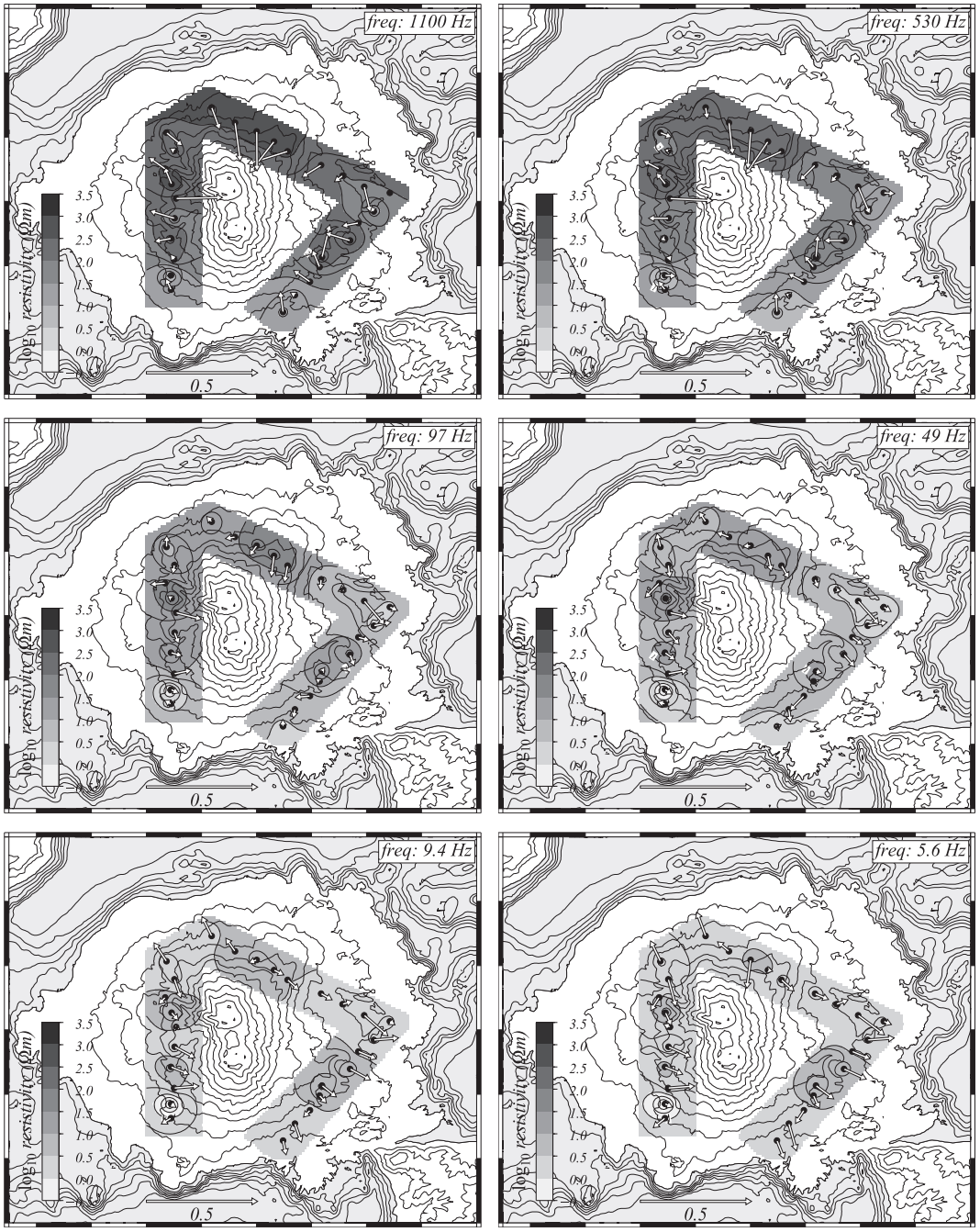

Fig. 3. Spatial distribution of apparent resistivity at frequencies (freq) of 1100, 530, 97, 49, 9.4, and 5.6 Hz. Apparent resistivity is calculated from det(Re(**Z**)), a rotational invariant of the magnetotelluric impedance tensor. White arrows denote the real parts of induction vectors (Parkinson's convention).

(Ogawa and Uchida, 1996) to the higher quality TM-mode data at ≥ 2 Hz along each measurement line. Topographic and bathymetric features were accounted for in the model, and the resistivity of seawater was fixed at 0.33 Ωm. Static shift was also included as an inversion parameter. The error floors for both the apparent resistivity and the phase were set at 5%. In Fig. 5(a), a 2-D resistivity section for the AK line is shown as an example inversion

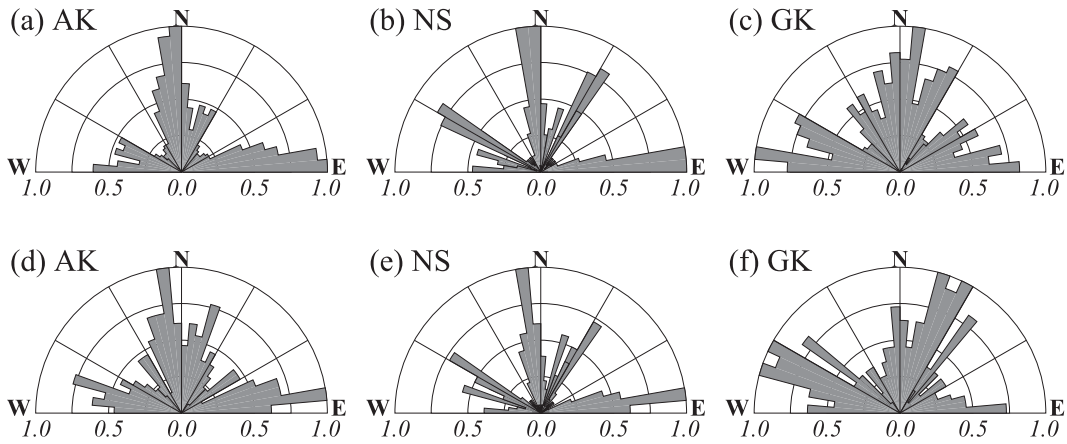

Fig. 4. Polar histograms of strike directions estimated from GBD results. Histograms of all frequency bands are shown for (a) AK line, (b) NS line, and (c) GK line, and those of lower frequency bands (＜10 Hz) are shown for (d) AK line, (e) NS line, and (f) GK line. Radial scale is normalized to enable comparative measurement between cases. Sector width is 5°. Note that strike directions have an intrinsic ambiguity about 90°.

result. The root mean square (RMS) error for the fits was 0.80. Pseudo-sections of the observed data and of the model responses are shown in Figs. 5(b) and (c). A significant number of the features in the observed data are reproduced by the inverted model.

The following features are seen in the resistivity structure. The first few hundred meters in depth along each line have high resistivities of between hundreds and thousands of ohm-meters. A non-uniform, heterogeneous layer with a low resistivity of less than 10 Ωm is then widely distributed below the surface layer. A resistive portion of less than 100 Ωm is also seen at high depths around the central zone of the AK line. Although the models fit the data well, the data corresponding to this deep high resistivity are not clear in the pseudo-sections. The resistive portions could be virtual images produced by inappropriate modeling of a 3-D structure by a 2-D analysis.

4. 3-D modeling

As we described in Section 3, 2-D interpretation of the entire dataset is inappropriate, because the correct strike directions cannot be assumed. As a result, a 3-D analysis was also conducted. To do this, we used a parallel implementation version of the WSINV3D code for 3-D inversion (Siripunvaraporn *et al*., 2005; Siripunvaraporn and Egbert, 2009). In the inversion, we used all four components of the impedance tensor (Z_{XX}, Z_{XY}, Z_{YX}, and Z_{YY}) as input data. The error floor was again set at 5%. Sixteen different frequencies were used in the calculation, chosen from observed frequencies between 2.03−3000 Hz such that the values had roughly equal spacing on the log scale.

To cover an area of 12 km × 12 km centered at Minamidake (hereinafter called the core area), a mesh length of 300 m was chosen. The core area encompassed almost all of the Sakurajima environs. Outside of the core area, the mesh size was enlarged by $\sqrt{2}$ times as the distance from the core area became large. Consequently, the number of horizontal mesh points was 62 in the E−W and N−S directions. In the vertical (depth) direction, the top 100 m was divided equally into 10 layers, and the thickness was then gradually enlarged with depth. The number of vertical mesh points was thus 41 from sea level to a depth of 53.3 km.

From consideration of the obtained 2-D models, the initial two-layer model (Model-U) was used: the first layer had a thickness of 100 m from the surface and a resistivity of 1000 Ωm, and the second layer was a uniform half-space with a resistivity of 100 Ωm. The seafloor topography was also sampled according to the above mesh, and was incorporated into the initial model. Resistivity blocks corresponding to seawater were fixed at 0.33 Ωm during the inversion process. Moreover, blocks containing both seawater and land was also fixed at a conductivity calculated from the weighted mean of the conductivities of land (10^{-3} or 10^{-2} S/m) and of seawater (3 S/m) according to the volume ratio. The topography on land was not taken into consideration in the modeling process, since the version of WSINV3DMT code used was unable to manage such information.

We first conducted a sensitivity test. Since our observation sites are distributed along the three lines on the flanks of Sakurajima, sensitivity to the conductor located beneath the central part of the volcanic edifice, which is away from the measurement lines, and to the conductor beneath one of the measurement lines was checked by

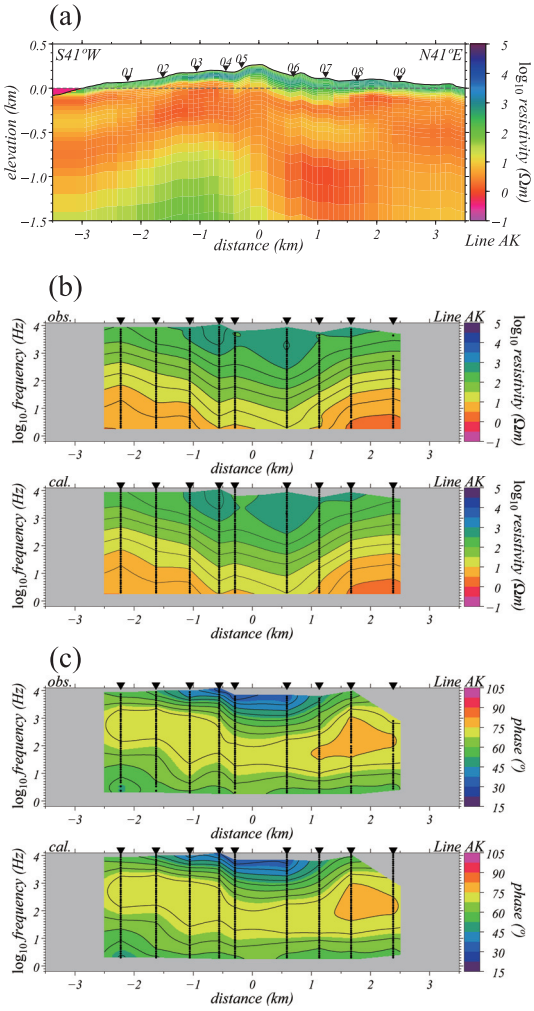

Fig. 5. (a) 2-D resistivity model profile for AK line. Inverted triangles denote AMT sites used for inversion (cf. Fig. 1). Horizontal dashed line indicates sea level. (b) Pseudo-sections for the observed (upper plot) and the calculated (lower plot) TM-mode apparent resistivity for AK line. (c) Pseudo-sections for the observed (upper plot) and the calculated (lower plot) TM-mode phase.

using three models shown in Fig. 6(a). Model-U is the initial model, which has a uniform second layer of 100 Ω m. Model-A and Model-B have conductive 1 Ωm regions A and B, respectively, in addition to Model-U. Region A corresponds to the conductor beneath the summit area and region B to that beneath the measurement line. The calculated curves of the apparent resistivity and the phase from the three models are shown for four sites in Fig. 6(b). Differences between Model-A (white dots) and Model-U (solid line) are seen in the phase curves of the observation sites nearest to the conductor (05 and 15) at around 10 Hz; however, the differences are as small as the error bars shown in the plots. The responses of sites 08 and 13 are mostly in agreement with those of Model-U. In contrast, notable differences between Model-B (gray dots) and Model-U are recognized in both the apparent resistivity and the phase curves at site 15 located right above the conductor and site 13 close to the conductor. On the basis of these results, we can conclude that little sensitivity is found to a conductive body located beneath the central part of the volcano, and that sufficient sensitivity is expected around the measurement line.

Fig. 7 shows a horizontal slice through the core area of the best-fit 3-D resistivity model, obtained as a result of inversion by using all the observation sites. After the RMS reached a sufficiently small value, a model with a smaller norm was searched for under a similar level of misfit (Siripunvaraporn *et al*., 2005). Consequently, the RMS error for this model is as low as 2.18; however, the match between the 3-D model and the non-diagonal components was less accurate at three sites to the south of the NS line (Fig. 8). This inaccuracy is due to the apparent resistivity values at site 18, which are about one order of magnitude smaller than those at surrounding sites. Since the phase curve at site 18 still maintains a similar profile, this discrepancy is regarded as a static shift (static shift correction was not applied in the 3-D study). To explain the low apparent resistivity data, a highly conductive body was placed in the model near to the surface at site 18 (Fig. 7), although the existence of this body is not practical for explaining the data at sites 17 and 19 (Fig. 8). Thus, the results indicate that static-shift correction is required even in 3-D modeling of AMT data.

Therefore, the inversion was conducted once more by removing the data for site 18 and using that for the other 26 observation sites. Four horizontal sections of the resultant final 3-D model are shown in Fig. 9. Moreover, typical examples of data-fits are shown for four sites in Fig. 10, and the RMS error of this model was 1.62. Although the response curves now reproduce the non-diagonal components well, at certain sites, the fit of the diagonal components of derived model and the data is inexact.

Features of the final model are summarized as follows. The resistivity close to the ground surface has high resistivity in general. Although nearly all areas in the vicinity of the measurement lines have high resistivity at a depth of 100 m (not shown), conductive portions are also seen both sides of the AK line and at the center of the NS line. At depths of 200−250 m, from the southern to the eastern region of Sakurajima the resistivity structure again becomes low. Finally, almost the entirety of Sakurajima has a resistivity of less than tens of ohm-meters at depths of 500−600 m, and this tendency continues at a depth of 1000 m. However, in an even deeper portion (～1500 m in depth) beneath the west half of the GK line, the resistivity

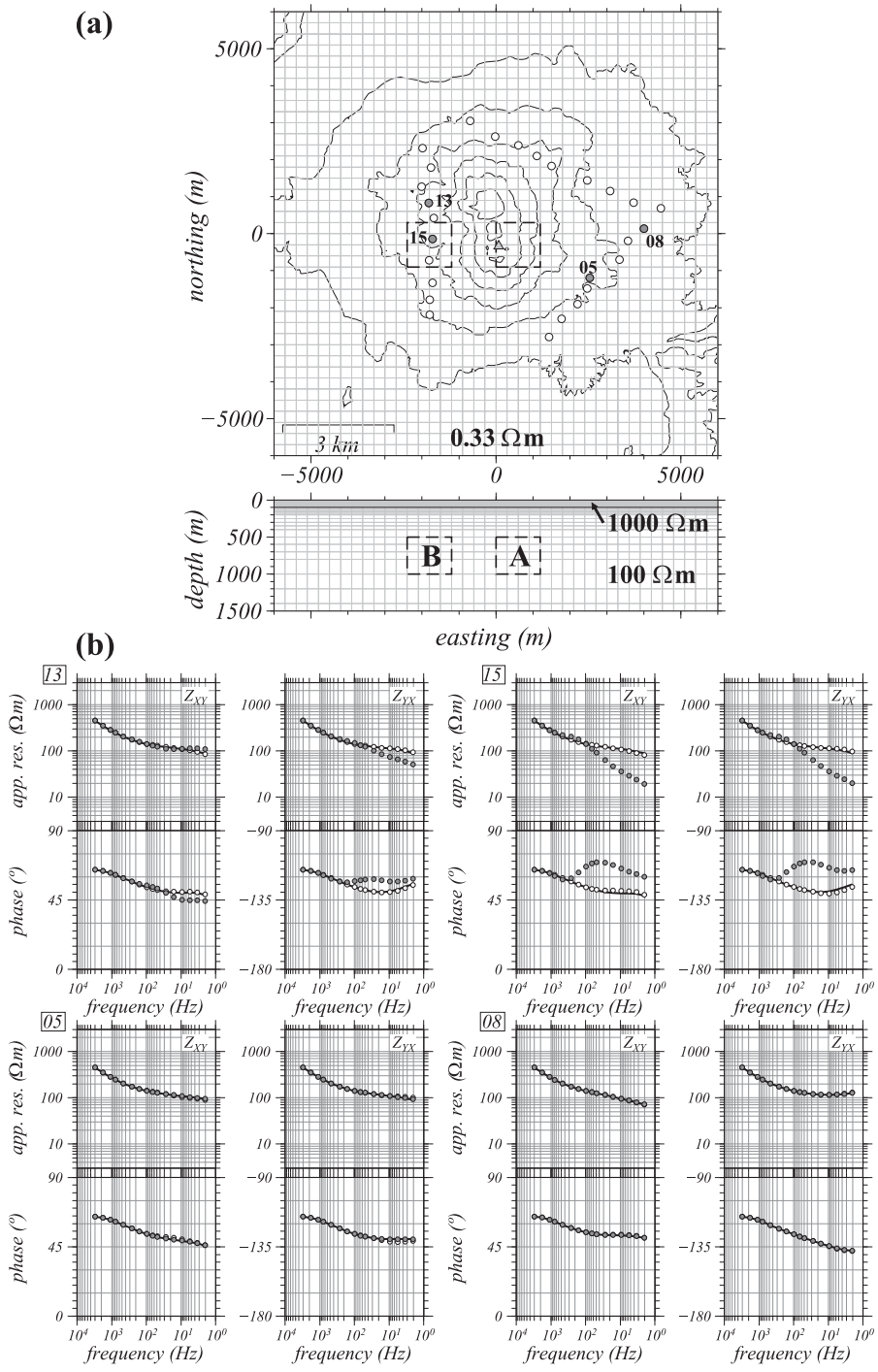

Fig. 6. (a) 3-D resistivity models used to perform sensitivity tests. Model-A has a prism-like conductor of 1 Ωm in region A in addition to the initial model (Model-U), and similarly for Model-B in region B. The size of both conductors is 1200 m × 1200 m (horizontal) × 500 m (vertical). Model-U is the initial model used for inversion. (b) Comparison of response curves of apparent resistivity (upper plot) and phase (lower plot), which are calculated from the non-diagonal components of impedance tensor, at four sites (site 13, 15, 05, and 08) for the three models. Solid lines indicate the responses of Model-U. White and gray dots denote the responses of Model-A and Model-B, respectively.

value increases and a high resistivity of hundreds of ohm-meters is found.

Since the topography was not incorporated into our model, the effect of the elevated center of the volcano, which may be included in the observed data, might have affected the inference of the 3-D structure. To estimate this effect, we calculated the responses of a simple model that incorporated the actual topography of Sakurajima by using another 3-D forward code (Mackie *et al.*, 1994). As a result, we found that the responses of the models (with and without the elevated center of volcano) mostly overlapped at the majority of the sites, although slight differences were seen at lower frequencies at a few sites located near the center of the measurement lines. The maximum deviation was 12 % (about 3 % on the log scale) in the apparent resistivity curve, and was 2.5 % in the phase curve. Because this maximum deviation in the apparent resistivity appeared at the lowest frequency calculated (1 Hz), we consider that the influence of the elevated center of the volcano on the final model (Fig. 9) is fairly limited.

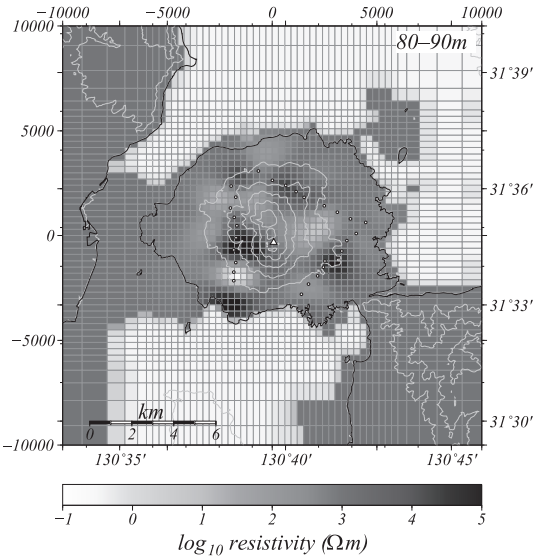

Fig. 7. Horizontal slice at depths of 80−90 m of best-fit 3-D resistivity model, obtained as a result of inversion using all the sites.

5. Discussion

5−1 Shallow structure near sea level

In Fig. 11, cross sections of the final model along the three measurement lines are shown. Since the topography was not incorporated into the model, the depth corresponding to sea level (simply the reverse of the 2-D topography along a measurement line) is drawn by a white dashed line. To interpret this 3-D model, we referred to borehole data from the Kurokami (KURB) and Harutayama (HARB) observation wells (Uto *et al*., 1999; Miki *et al*., 2000; Aizawa *et al.*, 2011).

KURB is a 381 m deep drilling well located 150 m east of site 08 (Fig. 1). According to the borehole lithology (Uto *et al*., 1999), the top 100 m is andesite lava effused from Nabe-yama in the 8th century, which is underlain by scoriaceous tuff breccia down to 240 m. Below this layer, lapilli tuff with pumice and block was found down to the bottom of the borehole. When compared with the obtained 3-D resistivity model around site 08 on the AK line (Fig. 11(a)), the boundary of the andesite lava coincides with the bottom surface of the high-resistivity layer. Therefore, this layer can be interpreted as being lava.

Next, the low resistivity of the second layer is considered. From temperature data logged for KURB, at the bottom of the lava layer a high temperature peak was found, and the temperature decreased as the depth increased into the underlain layers (Aizawa *et al.*, 2011). With the survey area close to the coastline before the Taisho eruption, we consider that cold seawater invaded

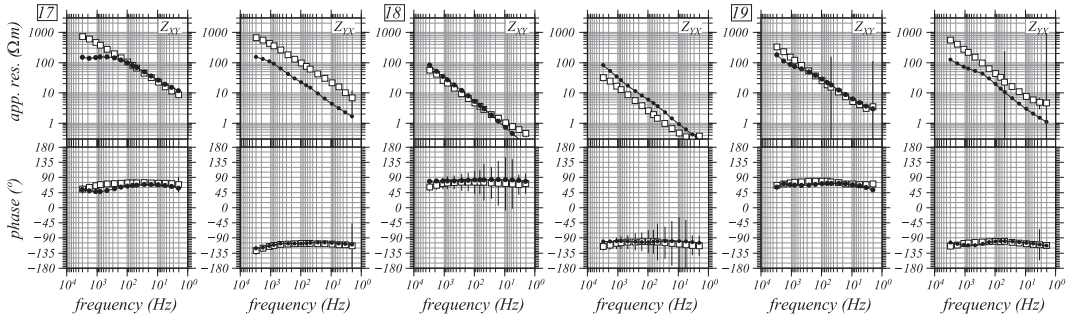

Fig. 8. Comparison between best-fit 3-D model from Fig. 7 and observed data. From left to right, Z_{XY}- and Z_{YX}-components are shown for three southern sites (17, 18, and 19) of the NS line. Open squares with error bars indicate the apparent resistivity (upper plots) and the phase (lower plots) used for 3-D inversion. Black dots with a solid line denote model responses.

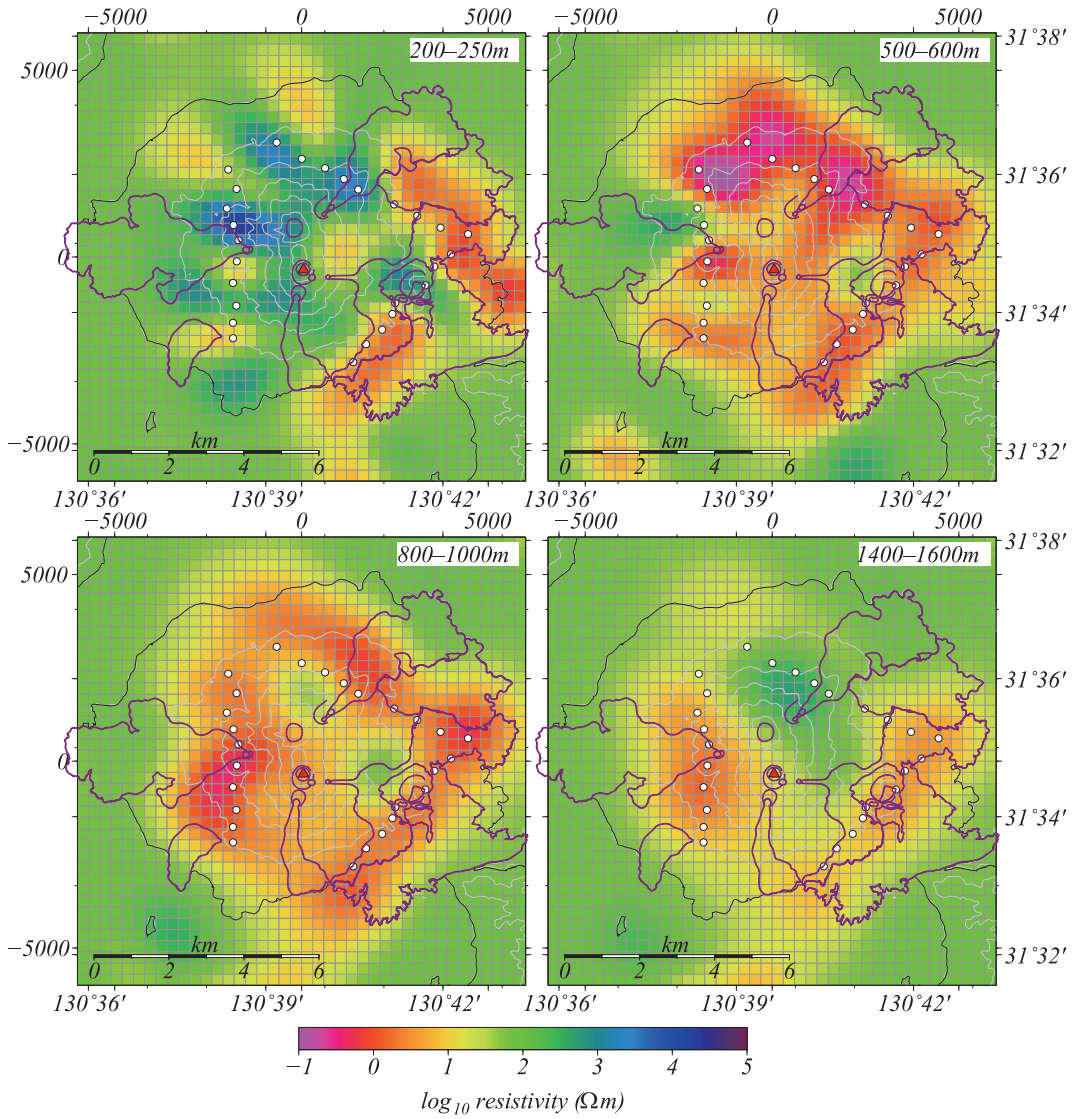

Fig. 9. Horizontal slices taken through the core area of the final 3-D model. Depths are indicated in the top-right corner of each plot. White dots denote AMT sites and the red triangle indicates the center of Minami-dake crater. Outlines of historical lava and craters (cf. Fig. 1) are also drawn with red lines.

into the second layer. That is, the conductive second layer can be interpreted as an aquifer including seawater or groundwater. For an area from the south of Sakurajima to the east, the obtained 3-D model can be explained primarily by this two-layer structure (Figs. 11(a) and (c)).

HARB is a 408 m deep borehole located 300 m southwest of site 12 and 500 m northwest of site 13 (Fig. 1). A top layer about 20 m in depth from the surface is occupied by recent ejecta such as volcanic ashes, and this is underlain by andesite lava of greater than 300 m in thickness (Miki *et al*., 2000). In the lower section of the borehole, tuff breccias appeared at about 50 m above sea level (asl), and groundwater is contained in this layer (Iguchi, 1987). If these geological features are compared with the resistivity structure of the NS line (Fig. 11 (b)), similar to KURB, the bottom of andesite lava correspond to the boundary between the first high-resistivity layer and the second conductive layer. Therefore, the first layer is again interpreted as a lava layer. From a comparison with the resistivity structure in the south and east area of Sakurajima (Fig. 11(a)), we clearly see that the andesite lava is distributed thickly.

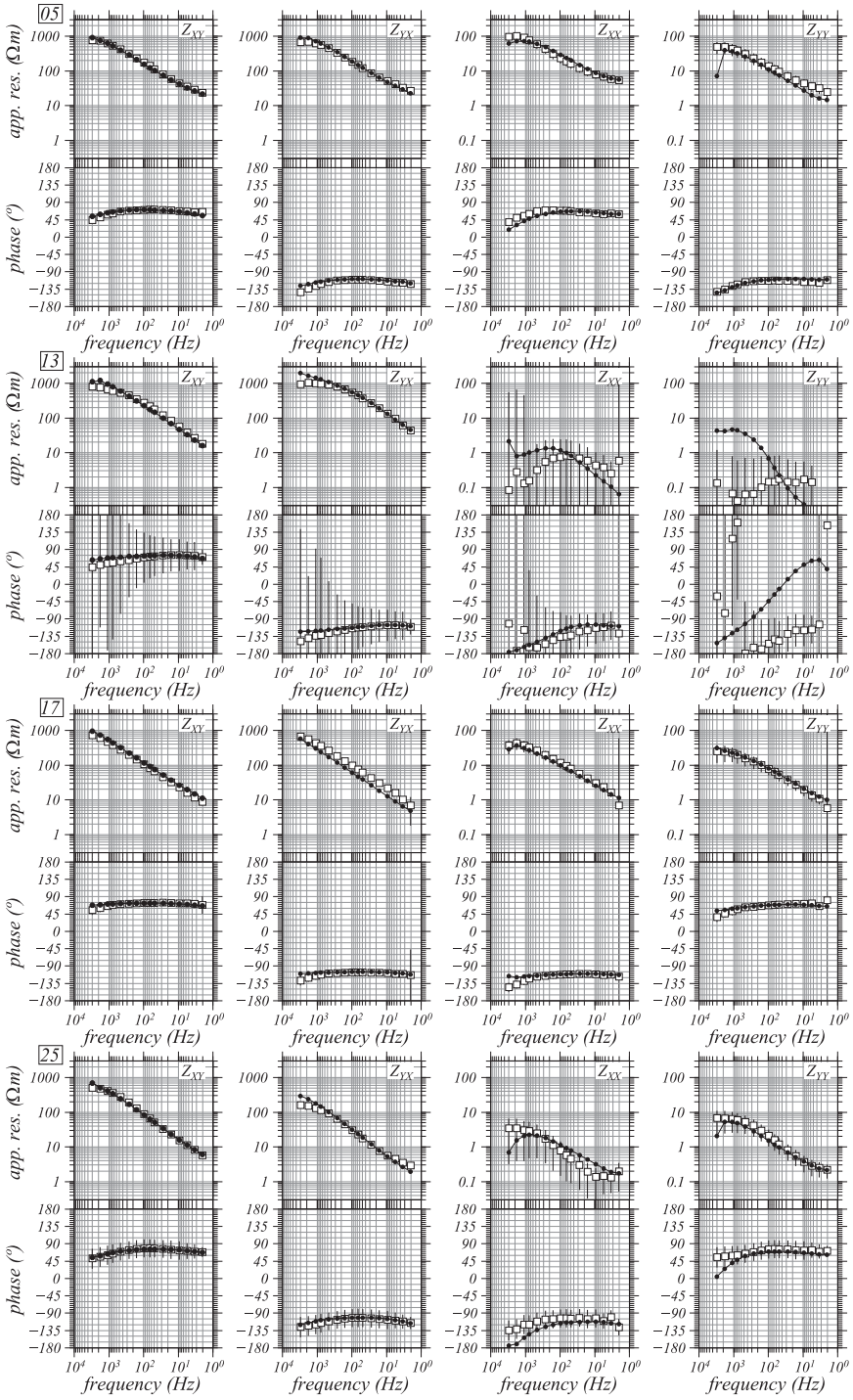

Fig. 10. Comparison between final 3-D model from Fig. 9 and observed data. From left to right, Z_{XY^-}, Z_{YX^-}, Z_{XX^-}, and Z_{YY^-} components are shown for four sites (05, 13, 17, and 25). Symbols are as in Fig. 8.

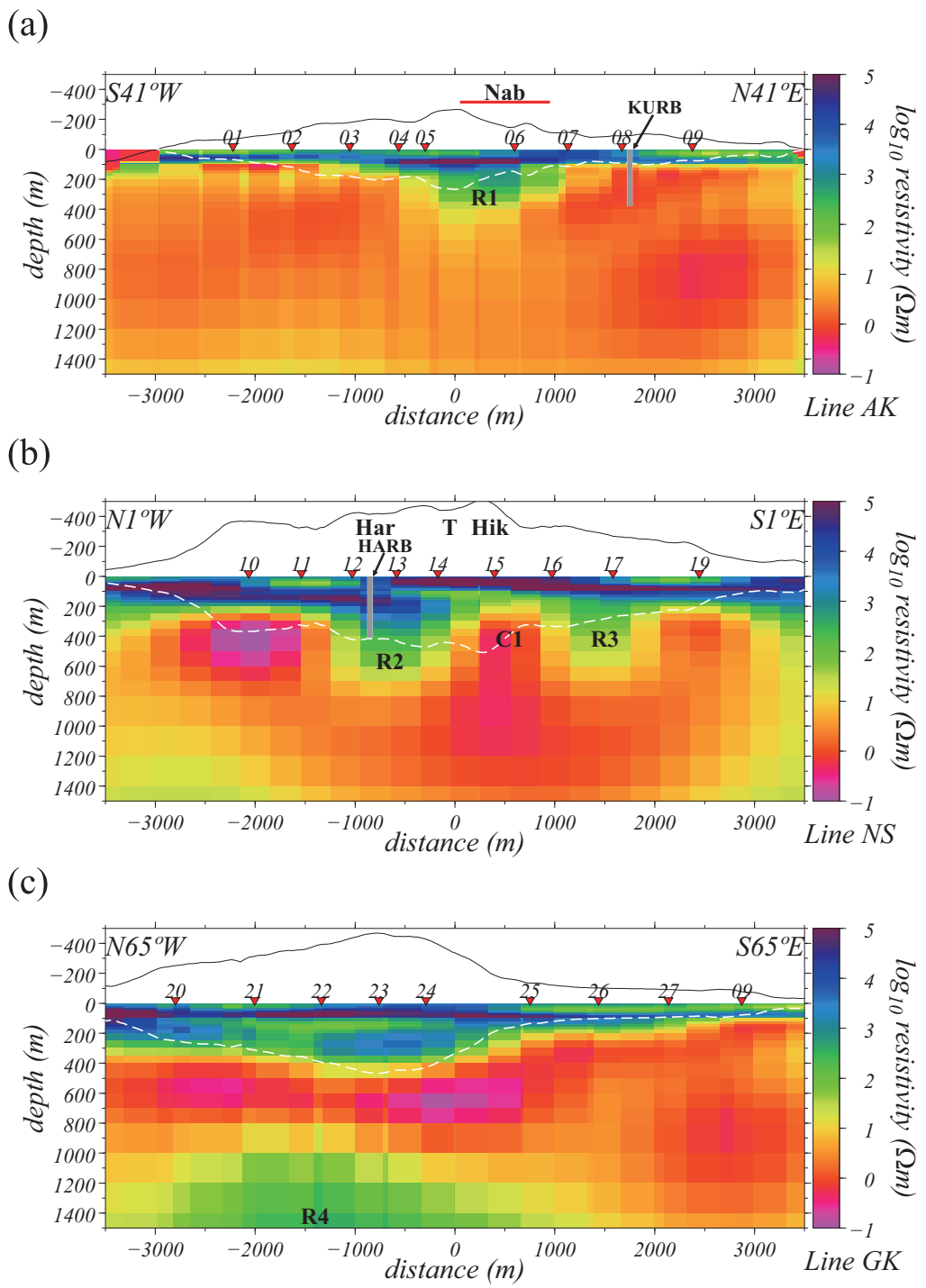

Fig. 11. Resistivity cross sections along measurement lines extracted from the final 3-D model: (a) AK line, (b) NS line, and (c) GK line. High-resistivity anomalies are labeled R1 to R4, while a conductive one is labeled C1. Black solid and white dashed lines indicate the topography of each profile and sea level, respectively. The vertical gray bar shows the location and depth of the borehole KURB in (a) and of HARB in (b). Labels for the geographical features are as in Fig. 1. Note that horizontal mesh intervals in the figures are not constant, because measurement lines are not in agreement with the direction of the horizontal mesh of 3-D model.

However, in the lower portion of this layer, the resistivity has a low value of around 100 Ωm. Along the GK line the surface resistive layer also shows a low value at depth (Fig. 11(c)). Given that HARB is close to the center of the volcano, while groundwater may be contained in the second layer, this layer can also be interpreted as a hydrothermally altered layer that prevents groundwater from penetrating into the deeper regions.

5−2 Basement structure

Komazawa *et al*. (2008) inferred the elevated basement structure situated from the west to south side of Sakurajima from an analysis of gravity data. Since the depth to the gravity basement along the NS line was about 500 m bsl, it was expected that the basement structure would be found by our AMT measurements. However, the depth of this gravity basement is equivalent to the low-resistivity second layer in the 3-D model (Fig. 11(b)).

Regarding the reason as to why the basement structure is not electrically clear, we consider two possibilities. The first is that the boundary between the second conductive layer and the underlain basement cannot be identified because the basement rock also has low resistivity. However, along the GK line, a high-resistivity zone of hundreds of ohm-meters is found at depths greater than 1000 m beneath sites 20 to 24 (R4 in Fig. 11(c)). This resistive zone is in agreement with the depth of the gravity basement proposed by Komazawa *et al*. (2008). A similar high-resistivity zone is detected by the 2-D model along the AK line at a depth of 1000 m underneath sites 1 to 5 (Fig. 5(a)). However, even though this also agrees with the gravity basement, a high-resistivity portion is not seen in the corresponding 3-D model (Fig. 11 (a)). If these results are taken into consideration, the basement may have a resistivity value in the hundreds of ohm-meters, but is likely to be located at the sounding depth or at an even deeper level.

The second possibility is that the actual basement is located at a position deeper than that proposed by Komazawa *et al*. (2008) in western Sakurajima. Aramaki (1977) stated that the 800 m class borehole located near the west coast of Sakurajima did not reach the basement rock (the Shimanto Group), and that the borehole was largely occupied by tuff corresponding to the Kekura formation found in the Satsuma Peninsula (Oki and Hayasaka, 1970). Yokoyama and Ohkawa (1986) proposed a model with a deeper gravity basement in light of this evidence. In the shallow-seismic-reflection-structure model for northeastern Sakurajima proposed by Tsutsui *et al*. (2011), the least reflective zone was found between the reflection horizon, identified as the basement, and sea level, and the zone was interpreted as being due to pyroclastic materials ejected from underwater eruptions. This zone was located between 100 and 800 m bsl and thus matches up with the second conductive layer. In addition, Oshima (2008) investigated the borehole data for Shirahama, on the northern coast, and for Hakamagoshi, near the western coast (Fig. 1), and reported that hot spring water was drawn from the Kekura formation layer at depths of between 900 and 1000 m for both wells.

These results are consistent with the hypothesis that the low-resistivity layer in western and northern Sakurajima corresponds to the Kekura formation layer. If sedimentary rocks of marine origin are widely distributed within Sakurajima, the second layer might have been affected by the highly conductive seawater, even in the western and northern areas.

5−3 Relation to flank eruptions

As seen so far, the shallow resistivity structure of Sakurajima consists of a high-resistivity surface layer that covers a thick conductive layer, and only part of the basement structure is clearly detected. The boundary between the first and second layers is situated approximately at sea level. However, in the areas labeled R1 on the AK line (Fig. 11(a)), and R2 and R3 on the NS line (Fig. 11 (b)), the conductive second layer found at depths below sea level. In contrast, near the Hikino-hira lava dome between R2 and R3, the second conductive layer is identified at a depth shallower than sea level (marked C1 in Fig. 11(b)).

R1 is located beneath the Nabe-yama pumice cone (Nab in Fig. 1) that was formed by eruptions in 764 (the Tenpyo-Hoji eruption). The majority of the craters that effused lava during the Taisho eruption in 1914 are located at the edge of Nabe-yama. Moreover, the Haruta-yama lava dome (Har in Fig. 1) and a further row of craters resulting from the Taisho eruption (T in Fig. 1) are situated near the ground surface above R2. These resistive zones are likely to be fracture zones related to the eruptive activity, in which groundwater is undersaturated. As regards R3, there is neither a corresponding crater nor a cone on the ground surface over which M4 lava from the prehistoric age (Fukuyama and Ono, 1981) has spread. With the Bunmei lava from 1476 southwest of R3, and the Miyamoto (M1) and Kannon-zaki lavas (M2) from 3000−4000 years ago (Miki, 1999), whose craters are unknown, to the east of the Bunmei lava (Fig. 1), R3 may be related to these eruptions.

Finally, C1 is considered. Various inconsistent data have been reported around C1 or to its north. High fluxes of soil CO_2 and R_n gases, which are considered to indicate the presence of hydrothermal fluids, were observed on Haruta-yama and Yuno-hira lava domes, although the flux of those gases was low on Hikino-hira and Taisho crater (Kusakabe and Hirabayashi, 1988; Hirabayashi *et al*., 2008). In addition, a positive anomaly of self-potential (SP) was reported around the Taisho crater (Hashimoto *et al*., 1998). Although the positive SP anomaly has been conventionally interpreted as an indication of the upward flow associated with hydrothermal circulation, recent studies suggest that a shallow high-conductivity zone enhances SP values around the summit area (Ishido, 2004; Aizawa *et al*., 2009). The

low CO_2 emissions and positive SP anomalies above a high-conductivity zone were also observed in the summit area at Stromboli volcano (Finizola *et al.*, 2006). These observational evidences can be explained by the model that the upper part of the hydrothermal zone is self-sealed by hydrologically impermeable and electrically conductive altered rocks (Aizawa *et al.*, 2009). Therefore, the upper part of C1 is likely to consist of such hydrothermally altered rocks, and a hydrothermal system has presumably developed underneath the altered zone. Conversely, the elevated second layer is not seen beneath craters located on the edge of Nabe-yama that erupted lava at the time of Taisho eruption. Despite the fact that 90 years or more have passed after the Taisho eruption, the heat source has still affected the shallow subsurface under the crater on the western flank, whereas evidence suggests that a heat source is not present beneath the eastern foot of Sakurajima.

6. Conclusions

We conducted an audio-frequency magnetotelluric survey at the foot of Sakurajima volcano in order to reveal the shallow region of the electrical resistivity structure. From the result of 3-D modeling, the heterogeneous resistivity structure beneath the flanks of Sakurajima, including the regions where lava effusion took place in past large-scale eruptions, was clarified for the first time. The following findings have been obtained.

(1) The shallow resistivity structure can be expressed by two layers: a high-resistivity layer corresponding to surface lava, and beneath this, a low-resistivity layer containing seawater/groundwater. The first lava layer is distributed thickly to the north and west of Sakurajima.

(2) The basement structure is not clearly detected, except for along a section of the GK line. The conductive second layer is distributed thickly over the entirety of Sakurajima, and is likely to correspond to the Kekura formation, a marine deposit layer.

(3) Although the boundary between the first and second layers is generally located at around sea level, beneath certain areas, such as the Haruta-yama lava dome and the Nabe-yama pumice cone, the conductive second layer is found at a deeper level. The fracture zone associated with previous eruptive activity is expected to be formed above this conductive layer.

(4) The conductive second layer is identified at a depth shallower than sea level nearby the Hikino-hira lava dome, suggesting that a hydrothermal system has developed underneath the vicinity of a crater row from the Taisho eruption and around Hikino-hira. Conversely, no elevation of the second layer is found close to the Taisho crater on the opposite side.

Acknowledgements

For assistance in implementing the AMT survey at Sakurajima, we express our gratitude to the Osumi Office of the River and National Highway and its Sabo Branch Office in Sakurajima, the Kagoshima District Forest Office, the Crisis Management Bureau of Kagoshima Prefecture, and the Safety Division of Kagoshima City. The staff at the Sakurajima Volcano Research Center of Kyoto University is also acknowledged for their cooperation and useful discussions. A number of discussions with Tomoki Tsusui of Akita University were fruitful for interpreting the electrical structure model of Sakurajima. Instruction concerning the use of the WSINV3DMT code (Siripunvaraporn and Egbert, 2009) from Songkhun Boonchaisuk of Mahidole University was very helpful. Our thanks also go to the two referees, T. Kagiyama and an anonymous one, and the Editor-in-Charge (M. Iguchi) for their constructive comments and suggestions to improve the manuscript. Numerical calculations were carried out on TSUBAME2.0 at the Global Scientific Information and Computing Center of Tokyo Institute of Technology. Most figures were prepared with General Mapping Tools (Wessel and Smith, 1991). This study was supported by the Japanese Ministry of Education, Culture, Sports, Science and Technology (MEXT), under the 7th National Project for Prediction of Volcanic Eruptions.

References

Aizawa, K., Ogawa, Y. and Ishido, T. (2009) Groundwater flow and hydrothermal systems within volcanic edifices: Delineation by electric self-potential and magnetotellurics. *J. Geophys. Res.*, **114**, B01208, doi: 10.1029/2008JB005910.

Aizawa, K., Kanda, W., Ogawa, Y., Iguchi, M., Yokoo, A., Yakiwara, H. and Sugano, T. (2011) Temporal changes in electrical resistivity at Sakurajima volcano from continuous magnetotelluric observations. *J. Volcanol. Geotherm. Res.*, **199**, 165–175.

Aramaki, S. (1977) Basement of Aira caldera and ejecta from Sakurajima volcano. In *2nd Joint observation of Sakurajima volcano* (Kamo, K. ed.), Sakurajima Volcanological Observatory, Kagoshima, 105–119 (in Japanese).

Bahr, K. (1988) Interpretation of the magnetotelluric impedance tensor: regional induction and local telluric distortion, *J. Geophys.*, **62**, 119–127.

Eto, T. (1967) Volcanic crustal deformation (III): crustal deformation in the vicinity of Aira caldera and the activity of Sakurajima volcano. *Bull. Volcanol. Soc. Jpn.*, **12**, 80–88 (in Japanese with English Abstract).

Eto, T., Takayama, T., Yamamoto, K., Hendrasto, M., Miki, D., Sonoda, T., Matsushima, T., Uchida, K., Yakiwara, H., Yenbin, W., Kimata, F., Miyazaki, R. and Kobayashi, K. (1997) Re-upheaval of the ground surface at the Aira caldera−December 1991～October 1996−. *Annual., Disas. Prev. Res. Inst., Kyoto Univ.*, **40 B1**, 49–60 (in Japanese with English Abstract).

Finizola, A., Revil, A., Rizzo, E., Piscitelli, S., Ricci, T., Morin, J., Angeletti, B., Mocochain, L. and Sortino, F. (2006) Hydrogeological insights at Stromboli volcano

(Italy) from geoelectrical, temperature, and CO_2 soil degassing investigations. *Geophys. Res. Lett.*, **33**, L17304, doi: 10.1029/2006GL026842.

Fukushima, H., Yamamoto, T., Nakaya, K., Sakai, H., Sugawara, H., Wakino, Y., Teshima, S., Ikeda, K. and Oowada, T. (1988) Electrical resistivity survey by using an ELF-MT method in Sakurajima. *Tech. Rep. Kakioka Magnetic Observatory*, **28**, 63−71 (in Japanese).

Fukushima, H., Yamamoto, T., Uwai, T., Ikeda, K. and Nakaya, K. (1989) Electrical resistivity survey by using an ELF-MT method in Sakurajima (2). *Tech. Rep. Kakioka Magnetic Observatory*, **29**, 139−142 (in Japanese).

Fukuyama, H. and Ono, K. (1981) **Geological map of Sakurajima Volcano**, 1: 25.000, **1**. *Geol. Surv. Jpn.* (in Japanese).

Groom, R. W. and Bailey, R. C. (1989) Decomposition of the magnetotelluric impedance tensor in the presence of local three-dimensional galvanic distortion. *J. Geophys. Res.*, **94**, 1913−1925.

Hashimoto, T., Tanaka, Y., Mogi, T., Nishida, Y., Ohba, S., Yamamoto, K. and Ishihara, K. (1998) Self-potential and hydrothermal system in the western part of Sakurajima volcano. *Annual., Disas. Prev. Res. Inst., Kyoto Univ.*, **41 B1**, 145−151 (in Japanese with English Abstract).

Hayasaka, S. (1987) Geologic structure of Kagoshima Bay, South Kyushu, Japan. *The Association for Geological Collaboration in Japan. Monograph*, **33**, 225−233 (in Japanese with English Abstract).

Hirabayashi, J., Nogami, K., Kakuage, Y., Iguchi, M. and Miki, D. (2008) Relationship between volcanic activity of Sakurajima and chemical composition of volcanic gases, and diffusion discharge of the carbon dioxide gas from the soil. In *10th Joint observation of Sakurajima volcano* (Ishihara, K. ed.), Sakurajima Volcanological Observatory, Kagoshima, 149−163 (in Japanese).

Iguchi, M. (1987) On the relation between "high-frequency acoustic waves" in the groundwater and volcanic activity of Sakurajima volcano. *Annual., Disas. Prev. Res. Inst., Kyoto Univ.*, **30 B-1**, 1−7 (in Japanese with English Abstract).

Iguchi, M. (2006) Aira Caldera storing magma. *Chikyu monthly*, **28**, 115−121 (in Japanese).

Iguchi, M., Yokoo, A. and Tameguri, T. (2010) Intensity of volcanic explosions at Showa crater of Sakurajima volcano. *Annual., Disas. Prev. Res. Inst., Kyoto Univ.*, **53 B**, 233−240 (in Japanese with English Abstract).

Ishido, T. (2004) Electrokinetic mechanism for the "W"-shaped self-potential profile on volcanoes. *Geophys. Res. Lett.,* **31**, L15616, doi: 10.1029/2004GL020409.

Ishihara, K. (1988) Geophysical evidences on the existence of magma reservoir and conduit at Sakurajima volcano, Japan. *Annual., Disas. Prev. Res. Inst., Kyoto Univ.*, **31 B-1**, 59−73 (in Japanese with English Abstract).

Japan Meteorological Agency (2005) **National catalogue of the active volcanoes in Japan (third edition)**. Japan Meteorological Business Support Center, Tokyo, 635p. (in Japanese).

Kagiyama, T. (2008) Eruption dominant volcanism vs. geothermal activitiy dominant volcanism: New aspect in volcanism. *J. Geotherm. Res. Soc. Jpn.*, **30**, 193−204 (in Japanese with English Abstract).

Kagiyama, T., Utada, H. and Yamamoto, T. (1999) Magma ascent beneath Unzen volcano, SW Japan, deduced from the electrical resistivity structure. *J. Volcanol. Geotherm. Res.*, **89**, 35−42.

Kamo, K. and Ishihara, K. (1980) Volcanic activity of Sakurajima viewed from the ground deformation. In *Report of Sakurajima area investigation committee*, Kagoshima Prefectural Government, Kagoshima, 19−27 (in Japanese).

Karohji, K., Nakaya, K., Sakai, H., Ikeda, K., Sugawara, M., Oowada, T., Fukushima, H., Yamamoto, T., Kato, Y., Kuwashima, M., Uwai, T., Tanaka, Y. and Masuda, H. (1989) Geo-electromagnetic observation in and around Sakurajima. In *7th Joint observation of Sakurajima volcano* (Kamo, K. ed.). Sakurajima Volcanological Observatory, Kagoshima, 47−58 (in Japanese).

Komazawa, M., Nakamura, K., Yamamoto, K., Iguchi, M., Akamatsu, J., Ichikawa, N., Takayama, T. and Yamazaki, T. (2008) Gravity anomalies at Sakurajima volcano, southwest Japan. *Annual., Disas. Prev. Res. Inst., Kyoto Univ.*, **51 B**, 261−266 (in Japanese with English Abstract).

Kubota, S., Koike, K., Ikeda, K.,Fukushima, H., Kumasaka, N., Wakino, Y., Teshima, S., Shimizu, Y., Yamamoto, T., Ishii, Y., Tanaka, Y. and Masuda, H. (1995) Geo-electromagnetic observation in and around Sakurajima. In *8th Joint observation of Sakurajima volcano* (Kamo, K. ed.), Sakurajima Volcanological Observatory, Kagoshima, 45−54 (in Japanese).

Kusakabe, M. and Hirabayashi, J. (1988) Distribution of soil R_n and monitoring of reduced gas concentration in an observation wall at Sakurajima. In *6th Joint observation of Sakurajima volcano* (Kamo, K. ed.), Sakurajima Volcanological Observatory, Kagoshima, 81−88 (in Japanese).

Mackie, R. L., Smith, J. T. and Madden, T. R. (1994) Three-dimensional electromagnetic modeling using finite difference equations: The magnetotelluric example. *Radio Sci.*, **29**, 923−935.

Miki, D. (1999) Estimate of the ages of lava flows at Sakurajima volcano, Kyushu, Japan; Inferred from paleomagnetic directions and paleointensities. *Bull. Volcanol. Soc. Jpn.*, **44**, 111−122 (in Japanese with English Abstract).

Miki, D., Uto, K., Uchiumi, S. and Ishihara, K. (2000) K-Ar dating and paleomagnetic measurements on drilled cores from the Sakurajima volcano: Part 1. *Annual., Disas. Prev. Res. Inst., Kyoto Univ.*, **43 B1**, 1−6 (in Japanese with English Abstract).

Müller, A. and Haak, V. (2004) 3-D modeling of the deep electrical conductivity of Merapi volcano (Central Java): integrating magnetotellurics, induction vectors and the effects of steep topography. *J. Volcanol. Geotherm. Res.*, **101**, 129−154.

Nishimura, S., Mogi, T. and Katsura, K. (1988) Electrical resistivity structure of Sakurajima volcano inferred from an ELF-MT method. In *6th Joint observation of Sakurajima volcano* (Kamo, K. ed.), Sakurajima Volcanological Obser-

vatory, Kagoshima, 73–79 (in Japanese).

Nishimura, S., Arsadi, E. M., Katsura, I., Yamada, Y., Mogi, T., Nishida, J. and Kusunoki, K. (1989) Electrical resistivity structure of Sakurajima volcano inferred from an ELF-MT and a CSA-MT methods. In *7th Joint observation of Sakurajima volcano* (Kamo, K. ed.), Sakurajima Volcanological Observatory, Kagoshima, 59–63 (in Japanese).

Ogawa, Y. and Uchida, T. (1996) A two-dimensional magnetotelluric inversion assuming Gaussian static shift. *Geophys. J. Int.*, **126**, 69–76.

Oki, K. and Hayasaka, S. (1970) Quaternary stratigraphy in the northern part of Kagoshima City. *J. Fac. Sci., Kagoshima Univ., Geol. Biol.*, **3**, 67–92 (in Japanese with English Abstract).

Oshima, H. (2008) Hydrological environment in the shallow part of Sakurajima volcano. In *10th Joint observation of Sakurajima volcano* (Ishihara, K. ed.), Sakurajima Volcanological Observatory, Kagoshima, 191–193 (in Japanese).

Parkinson, W. D. (1962) The influence of continents and oceans on geomagnetic variations. *Geophys. J. R. Astr. Soc.*, **6**, 441–449.

Reid, M. E. (2004) Massive collapse of volcano edifices triggered by hydrothermal pressurization, *Geology*, **32**, 373–376.

Siripunvaraporn, W., Egbert, G., Lenbury, Y. and Uyeshima M. (2005) Three-dimensional magnetotelluric inversion: data-space method. *Phys. Earth. Planet. Interiors*, **150**, 3–14.

Siripunvaraporn, W. and Egbert, G. (2009) WSINV3DMT: Vertical magnetic field transfer function inversion and parallel implementation. *Phys. Earth. Planet. Interiors*, **173**, 317–329.

Szarka, L. and Menvielle, M. (1997) Analysis of rotational invariants of the magnetotelluric impedance tensor. *Geophys. J. Int.*, **129**, 133–142.

Tanaka, Y., Masuda, H., Yukutake T., Kawamura M., Mizuno Y., Nagano, T., Baba, H., Ikeda, K. and Fukushima H. (1982) Electrical resistivity measurement using a bipole-dipole method in Sakurajima. In *4th Joint observation of Sakurajima volcano* (Kamo, K. ed.), Sakurajima Volcanological Observatory, Kagoshima, 59–67 (in Japanese).

Tanaka, Y., Masuda, H., Yukutake T., Kawamura M., Nagano, T., Nakaya, K., Toya, T. and Ikeda, K. (1986) Electrical resistivity observation in Sakurajima. In *5th Joint observation of Sakurajima volcano* (Kamo, K. ed.), Sakurajima Volcanological Observatory, Kagoshima, 61–69 (in Japanese).

Tokumoto, T., Nakaya, K., Fukushima, H., Sugawara, M. and Sakai, H. (1988) Measurement of the electrical resistivity in Sakurajima. *Tech. Rep. Kakioka Magnetic Observatory*, **27**, 38–43 (in Japanese).

Tsutsui, T., Imai, M., Tsushima, K., Yagi, N., Iguchi, M. and Tameguri, T. (2011) The shallow seismic reflection structure in the northeastern part of the Sakurajima volcano with the pseudo-reflection method. *Bull. Volcanol. Soc. Jpn.,* **56**, 201–212 (in Japanese with English Abstract).

Uto, K., Miki, D., Uchiumi, S. and Ishihara, K. (1999) K-Ar dating and paleomagnetic measurements on drilled cores from the Sakurajima volcano. *Annual., Disas. Prev. Res. Inst., Kyoto Univ.*, **42 B1**, 27–34 (in Japanese with English Abstract).

Wessel, P. and Smith, W. H. F. (1991) Free software helps map and display data. *EOS Trans. AGU*, **72**, 445–446.

Yamazaki, A., Toyodome, S., Ito, N., Ikegame, T., Iwase, Y., Kumagai, Y. and Muromatsu, F. (1998) Geo-electromagnetic observation in and around Sakurajima. In *9th Joint observation of Sakurajima volcano* (Ishihara, K. ed.), Sakurajima Volcanological Observatory, Kagoshima, 79–90 (in Japanese).

Yokoyama, I. and Ohkawa, S. (1986) The subsurface structure of the Aira caldera and its vicinity in southern Kyushu, Japan. *J. Volcanol. Geotherm. Res.*, **30**, 253–282.

Yukutake, T., Yoshino, T., Utada, H., Kawamura M., Nagano, T., Kato, Y., Baba, H., Nakaya, K., Tanaka, Y. and Masuda, H. (1980) Electrical resistivity measurement in Sakurajima. In *3rd Joint observation of Sakurajima volcano* (Kamo, K. ed.), Sakurajima Volcanological Observatory, Kagoshima, 55–62 (in Japanese).

(Editorial handling Masato Iguchi)

AMT 観測から推定される桜島火山の浅部比抵抗構造

神田　径・山崎友也・小川康雄・橋本武志・坂中伸也・相澤広記・
高倉伸一・小山崇夫・山田健太・小林　宰・小森省吾

2007 年 11 月，第 7 次火山噴火予知計画の一環として，桜島火山の山麓で AMT 法比抵抗構造調査を実施した．南岳山頂火口および昭和火口では，ブルカノ式噴火が繰り返し発生するため，山頂付近へ近づくことができない．そこで我々は，山体の北，西，南東山麓にそれぞれ測線を設定し，合計 27 観測点で周波数 1～10400 Hz の電磁場データを取得した．データは，2 Hz 以上の周波数帯で概ね良好であった．まず，各測線で得られたデータに対して 2 次元解析を行った．しかしながら，インピーダンスから推定される構造走向は，全ての測線においてほぼ南北方向を示し，2 次元解析は不適当であることが判明したことから，全てのデータを矛盾なく説明するために，3 次元解析を行った．3 次元モデリングの結果明らかとなった桜島の浅部比抵抗構造は，以下のような特徴を持つ．表層は溶岩層に対応する高比抵抗層で数百から数千Ωm の比抵抗値を示す．その下には，海水や地下水を含む層であると解釈される数Ωm 以下の低比抵抗層が続く．基盤構造は，桜島の北部の一部を除いて明瞭ではなく，2 層目の低比抵抗層が厚く分布している．表層の高比抵抗層と 2 層目の低比抵抗層との境界は，概ね海水準付近にあるが，ハルタ山溶岩ドームや鍋山軽石丘などの一部地域の下では，海水準より下に位置する．それらの地域では，過去の噴火に関係した破砕帯が形成されていると考えられる．また，引ノ平溶岩ドームから大正火口にかけての地下では，逆に低比抵抗層が地表近くまで盛り上がっており，熱水系の存在が示唆された．一方で，同じ大正噴火の際に溶岩流を流出させた鍋山の縁に位置する火口付近では，そのような低比抵抗層の盛り上がりは見られず，既に熱源が存在しないことを暗示している．